INTERNATIONAL JOURNAL FOR NUMERICAL METHODS IN FLUIDS, VOL. 20, 1215–1236 (1995)

NUMERICAL MODELLING OF CONFINED FLOW PAST A CYLINDER OF SQUARE CROSS-SECTION AT VARIOUS ORIENTATIONS

GUOPING LI AND JOSEPH A. C. HUMPHREY*

Thermofluids Laboratory, Department of Mechanical Engineering, University of California at Berkeley, Berkeley, CA 94720, U.S.A.

SUMMARY

Results are presented for the unsteady, two-dimensional flow and heat transfer due to a square obstruction of diameter d located asymmetrically between the parallel sliding walls of a channel with length-to-height ratio $W/H = 6{\cdot}44$. Analysis is based on the numerical solution of spatially and temporally second-order accurate finite difference approximations of the transport equations expressed in curvilinear co-ordinates. Laminar, constant property flow is assumed for obstruction configurations in which the blockage ratio is $d/H = 0{\cdot}192$, the nearest-wall distances are $g/d = 0{\cdot}2$, $0{\cdot}5$ and 1, the orientation angles are $\alpha = 0°$, 10° and 20° and the Reynolds numbers are $Re = 100$, 500, and 1000. Preparatory testing of the numerical procedure was performed for a variety of documented flows to verify its physiconumerical accuracy and obtain estimates of the residual grid-dependent uncertainties in the variables calculated. Heat transfer, drag and lift coefficients and Strouhal numbers for the present flow were finally calculated to within 4%–7% of their grid-dependent values using non-uniformly spaced grids consisting of ($x = 99$, $y = 55$) nodes. Above a critical value of the Reynolds number, which depends on the geometrical parameters, the flow is characterized by alternate vortex shedding from the obstruction top and bottom surfaces. Streamline, vorticity and particle streakline plots provide qualitative impressions of the unsteady vortical flow. Especially noteworthy are the extremes in the lift coefficient which ranges from large positive values for an obstruction with $g/d = 0{\cdot}2$ and $\alpha = 10°$ to negative values for one with $g/d = 0{\cdot}5$ and $\alpha = 0°$. Both the drag and lift coefficients as well as the Strouhal number exhibit non-monotonic variations with respect to the parameters explored. Asymmetries in the obstruction location and orientation account for relatively large vortex-induced periodic variations in heat transfer, especially along the wall nearest the obstruction. Notable differences are also predicted for the heat transfer coefficients of the individual obstruction surfaces as a function of the orientation angle.

KEY WORDS square obstruction; channel flow; vortex shedding; sliding walls; numerical calculation

1. INTRODUCTION

1.1. The problem of interest

The motion of a fluid past an immobile cylindrical obstruction with its longitudinal axis aligned normal to the approaching flow is of fundamental interest and considerable practical importance. Bluff body cross-flow configurations of this type arise in numerous industrial applications and

* Author to whom correspondence should be addressed. Present address: Department of Aerospace and Mechanical Engineering, University of Arizona, Tucson, Arizona 85721, U.S.A.

CCC 0271–2091/95/111215–22

Received 28 August 1992
Revised 31 August 1993

environmental settings, including: the passages in equipment used for heat and mass transfer processes; flow-metering devices; the cooling of electronic components and equipment; the obstructed spaces between co-rotating disks in magnetic disk storage devices; moving ground vehicles; tall buildings and structures such as chimneys, cooling towers, electrical pylons and offshore oil rigs. Bluff-body-induced flow unsteadiness and mixing can be used to advantage to enhance heat and mass transfer to or from the bluff body and/or its surroundings. However, the same flow unsteadiness gives rise to fluctuating drag and lift forces which can stress the body by making it vibrate. For example, together with fluctuating temperatures, the latter situation represents a potentially disastrous condition for the tubes in a heat exchanger tube bank. Similarly, flow-induced vibrations may seriously impair the read/write performance of a magnetic disk storage device.

Aside from the above practical motivating factors, the unsteady flow and heat transfer associated with cylindrically shaped bluff bodies are interesting in their own right and have been the subject of considerable basic research. In these studies the principal objective has been to measure and/or calculate the field variables and related quantities from which to determine cylinder drag and lift coefficients as well as Strouhal and Nusselt numbers. The studies can be classified according to the number, arrangement and cross-sectional shapes of the cylinders, the character of the approaching flow (laminar or tubulent) and whether it is of a free-stream or confined type. Most of the flow and heat transfer work reported in the literature pertains to single cylinders of circular or rectangular cross-section immersed in freestreams at both low and high speeds. Useful reviews have been compiled by Marris,[1] Berger and Wille[2] and Morgan.[3] Subsequently, noteworthy investigations have been performed by, among others, Davis and Moore,[4] Okajima,[5] Braza *et al.*,[6] Igarashi,[7,8] Franke *et al.*,[9] Gresho and Chan,[10] Cheng *et al.*,[11] Rodi,[12] Okajima *et al.*,[13] Karniadakis and Triantafyllou[14] and Kato and Launder.[15] A single study, by Vickery,[16] provides measurements of lift and drag RMS fluctuations as a function of the angular orientation of a cylinder of square cross-section immersed in a high-speed turbulent flow. That author shows that an angle of attack $\alpha > 15°$ can reduce the RMS of the lift fluctuations by an amount ranging between 50% and 73% depending on the turbulence level of the approaching flow.

The present study concerns cylinders in *confined* cross-flow configurations. Specifically, it concerns the numerical calculation of the unsteady streamlined motion of a fluid flowing past a single immobile cylinder of square cross-section located between the parallel walls of a two-dimensional channel, with the longitudinal axis of the cylinder aligned parallel to the channel walls and normal to the approaching flow. For conciseness, the two-dimensional geometry of interest is drawn in Figure 1. This shows that the cylinder location h/H and its angular orientation with respect to the horizontal, α, are both variable and that the channel walls may slide in the direction of the approaching flow at speed U_w. (The sliding wall condition is especially relevant to the aerodynamics of ground vehicles and magnetic disk drives.)

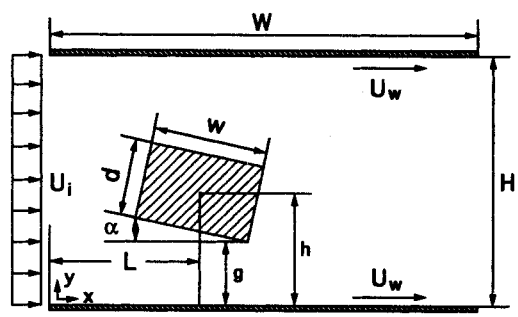

Figure 1. Schematic of the two-dimensional flow configuration of interest. In this work $w/d = 1$ and $U_w/U_i = 1$

Because of these three conditions, the bulk of the work performed to date on cylinders in free and confined flow configurations has but limited applicability to the present problem. A review of relevant information is summarized next, with additional details provided in Reference 17.

1.2. Related earlier work

In comparison with the freestream case, there is significantly less work on the flow and heat transfer for cylinders in confined cross-flow configurations. Bearman[18] has reviewed much of the earlier literature on related flow configurations pertaining to obstructions near stationary and sliding walls; the majority of the citations are experimental and correspond to turbulent, three-dimensional unsteady flows. Subsequently, in a series of detailed experiments, Marumo *et al.*,[19,20] H. Suzuki *et al.*,[21] and K. Suzuki *et al.*,[22] have systematically investigated the enhanced transport of heat through a turbulent boundary layer developing along a fixed flat wall perturbed by a single cylinder of circular cross-section located at different distances from the wall. These experimental studies show that, combined, the acceleration of fluid through the cylinder–wall gap and the overall (cylinder-induced) flow unsteadiness are responsible for marked increases in the heat transfer coefficient along a significant portion of the wall downstream of the cylinder. Similar fluid mechanics investigations ranging from $Re = 70$ to 3×10^4, approximately, have been performed by Taneda,[23] Bearman and Zdravkovich[24] and Kamemoto *et al.*[25] The latter two studies show that vortex shedding from the obstruction is significantly suppressed for cylinder–wall gap sizes $d/g < 0{\cdot}3$. While these investigations have focused on understanding the complicated cylinder–wall momentum and heat transport interactions, because they are primarily for circular cylinders in semiconfined turbulent boundary layer flows, the results are mostly of qualitative relevance to the present work.

Studies involving more than one cylinder arranged in a channel with fixed walls, such as two in tandem or a periodic array, have been performed by, for example, Karniadakis *et al.*,[26] Yao *et al.*,[27] Amon and Mikic,[28] Treidler[29] and Tatsutani *et al.*[30] In particular, Karniadakis *et al.*[26] show that cylinder-induced low-Reynolds-number flow instabilities of a *non-turbulent* nature produce channel wall heat transfer rates comparable with those of turbulent flows in unobstructed channels while incurring significantly less dissipation. This finding is of special interest to the present study and therefore a careful consideration of the work performed in channel flow configurations involving unsteady but streamlined fluid motion past single cylinders is appropriate. Table I summarizes the parameter ranges explored in three especially relevant investigations which are discussed next.

Table I. Summary of the parameter ranges investigated numerically in three cylinder–channel flow configurations especially relevant to the present work. Refer to Figure 1 and the Appendix for the definition of symbols. In the study of Davis *et al.*,[31] 87% of the grid was contained in a section of the channel with $W/H = 4$

Authors	α	h/H	g/d	d/H	w/d	W/H	U_w/U_i	Re
Davis *et al.*[31]	0°	0·5	2·5	0·167	0·6	∞	0	50–925
			1·5	0·250	1·0			
					1·7			
Suzuki *et al.*[32]	0°	0·5	9·5, 4·5	0·05, 0·1	1	12	0	37·5–150
			2·0, 1·17	0·2, 0·3				
			0·75, 0·50	0·4, 0·5				
Arnal *et al.*[33]	0°	0·03125	0	0·0625	1	2·5–5	0, 1	50–2000
Present work	0°	0·135	0·2	0·192	1	6·44	1	100
	10°	0·192	0·5					500
	20°	0·288	1·0					1000

In an extension of earlier work on freestream flows, Davis *et al.*[31] studied the flow past single cylinders of rectangular cross-section located on the centreline of a two-dimensional channel with fixed walls. Both measurements and calculations were performed in the Reynolds number range $50 < Re < 925$. The authors found good correspondence, ranging from about 4% to 13%, between the measured and calculated non-monotonic variations in the Strouhal number St as a function of Re. For both the blockage ratios examined, $d/H = 0{\cdot}167$ and $0{\cdot}250$, they observed that St initially increases sharply with Re up to $Re = 250$–300, as of which St slowly decreases with further increases in Re. They show that (for fixed Re) St increases with increasing blockage ratio d/H and that it is larger for the case of a uniform inlet channel profile than for one parabolic in shape. Similarly, the average drag coefficient was found to increase with increasing Re and increasing d/H and was larger for a uniform inlet velocity profile than for a parabolic one. The variations in the instantaneous lift and drag coefficients calculated for cylinder aspect ratios $w/d = 0{\cdot}6$, $1{\cdot}0$ and $1{\cdot}7$ at $Re = 125$ were described by simple sinusoids, but for $w/d = 1$ and $Re = 500$ they displayed more complex variations. Comparisons between calculated and visualized streaklines in the wake of the cylinder with $w/d = 1$ showed good qualitative agreement for values of $Re = 125$–145 (with $d/H = 1/6$), 250–275 (with $d/H = 1/4$) and 500–550 (with $d/H = 1/4$). Unsteady recirculating flow regions were predicted along both channel walls downstream of the cylinder for the cases with $w/d = 1$, $d/H = 1/4$ and $1/6$ at $Re = 500$.

In an investigation very similar to that of Davis *et al.*,[31] Suzuki *et al.*[32] visualized and calculated the unsteady two-dimensional flow past a square cylinder in a channel with fixed walls. The Reynolds number range explored was $37{\cdot}5 < Re < 150$ and, as in Reference 31, uniform and parabolic inlet flow profiles were investigated. The ranges of the geometrical parameters are given in Table I. One calculation with $d/H = 0{\cdot}3$ and $Re = 150$ was performed for $h/H = 0{\cdot}45$, $0{\cdot}325$ and $0{\cdot}2$ to investigate the effect on the flow due to changing the cylinder location relative to the channel walls. Another with $h/H = 0{\cdot}5$ and $d/H = 0{\cdot}3$ at $Re = 150$ involved sliding walls. Regrettably, neither set of results was discussed in depth. Many of the features predicted by the authors for the other flow configurations are qualitatively similar to those calculated by Davis *et al.*[31] However, the following additional findings are noted. The flow visualization results confirmed the assumed two-dimensionality of the flow up to $Re = 150$ or, equivalently, $Re_H = 500$. Both the visualized and calculated flow patterns revealed that, for all values of $d/H > 0{\cdot}1$ for which shedding occurred, the vortices alternately shed from the cylinder exhibited a 'criss-crossing' behaviour with respect to the channel centreline as the fluid moved downstream. This effect is also present in the calculatiolns of Davis *et al.*[31] and was observed even earlier in the flow visualization study of Zdravkovich.[34] For the case with $d/H = 0{\cdot}3$ the wall regions of the channel flow were noticeably disturbed by the vortices shed from the cylinder.

The two-dimensional flow past an immobile cylindrical obstruction of square cross-section placed immediately adjacent to one of the two walls of a channel, for both fixed and sliding walls conditions, has been investigated numerically by Arnal *et al.*[33] Eight values of the Reynolds number were calculated for the parameter ranges listed in Table I. Numerical tests led the authors to conclude that the imposition of a non-reflecting wave boundary condition at the exit plane and the use of non-uniform grids ranging between (113, 37) and (131, 37) nodes were sufficient to resolve the flow cases explored to better than 16% for the average drag coefficient and 1% for the Strouhal number. (Note that the Strouhal number in Reference 33 is incorrectly defined in their equation (10). This should read $St = fH/U_B$, where H is the cylinder diameter and U_B is the inlet flow velocity.) The grid Reynolds number in these calculations ranged between $Re_\Delta = 5$ and 100 approximately. As in References 31 and 32, calculations were also performed for the case of a square cylinder in freestream flow.

Among the authors' main findings for the sliding wall case are the following. For $Re < 100$ the flow field solutions were steady. At $Re = 100$ a mild flow unsteadiness was observed in the wake of the square cylinder. Periodic shedding of positive and negative vortices occurred somewhere between $Re = 100$ and 250. Relative to a square cylinder in a freestream, the presence of a sliding wall increased

the critical Reynolds number at which the flow became unsteady while simultaneously stabilizing the resulting unsteady flow in a strongly periodic motion. The same stabilization phenomenon has been observed experimentally by Taneda[23] for the case of a circular cylinder towed along the fixed wall of a channel. Arnal *et al.*[33] attribute the stabilization of periodic motion to the positive vorticity generated in the wall–cylinder corner immediately behind the cylinder (when the wall slides from left to right as in Figure 1), an effect of special importance to this work. Calculations of the cylinder drag coefficient for the sliding wall case showed that, as for the freestream case, this quantity increases with increasing Re but its magnitude is 60%–80% larger in the range $100 < Re < 1000$. Also, relative to the freestream case, the sliding wall had the effect of reducing the cylinder Strouhal number by as much as 45% in the same range of Reynolds number.

This section concludes with the following general observations for cylinders of square cross-section in the parameter ranges $100 < Re < 1000$ and $0 < d/H < 0{\cdot}25$.

(1) Relative to a square cylinder in a freestream, at all Re the Strouhal number, St, and the average drag coefficient, $\bar{C}_D$, for an identical cylinder located *symmetrically* on the centreline of a channel with fixed walls are both larger by amounts directly proportional to the obstruction ratio d/H. For both the freestream and fixed channel wall cases the respective $\bar{C}_D$ coefficients increase parabolically with Re. St initially increases sharply up to $Re = 250$–300, as of which point it decreases slowly with further increases in Re.

(2) For a pair of square cylinders placed immediately adjacent to the walls of a channel such that they face each other symmetrically, with $d/H = 0{\cdot}0625$ for each cylinder, the following may be said. For both the fixed and sliding wall conditions St is significantly smaller and $\bar{C}_D$ significantly larger than for the freestream case. For comparable values of d/H the drag on a cylinder immediately adjacent to the sliding wall of a channel can exceed by a factor of $1{\cdot}5$ that corresponding to a fixed wall condition. For both fixed and sliding wall conditions there is a critical value of Re, depending on the geometrical parameters, which marks the transition between steady and unsteady flows.

(3) Experimental evidence supports the notion of two-dimensional flow past a square cylinder in a channel with fixed walls up to at least $Re = 150$. However, it is known that the wakes of circular cylinders and bluff bodies in free streams undergo a transition from two-dimensional streamlined motions at $Re = 200$ to three-dimensional turbulent motions at $Re = 400$.[14] In the notable absence of any indications to the contrary, here it is tacitly assumed that the three-dimensionality which develops *downstream* of a cylinder in cross-flow has a negligible influence on space- and time-averaged quantities (such as drag and lift coefficients and Nusselt numbers) for the cylinder itself or the sections of the channel walls near it.

1.3. Objective of this investigation

From the above review it appears that little is known about the flow past single immobile cylinders of rectangular cross-section in channels with parallel sliding walls. The work of Arnal *et al.*[33] points to significant variations in the Strouhal number as well as the drag and lift coefficients for a square cylinder placed immediately adjacent to the sliding wall of a channel. However, the centreline symmetry plane boundary condition used by those authors implies the presence of *two* cylinders facing each other in the channel, a configuration differing significantly from the asymmetrical one of interest here. In addition, none of the cylinder–channel studies reviewed above includes thermal effects. Thus the respective influences on the flow and heat transfer due to varying the location and angular orientation of a cylinder relative to the sliding walls of a channel remain essentially unexplored.

The main objective of the present study has been to conduct a numerical investigation of these effects for forced convection flow conditions. The non-Cartesian nature of the flow configuration, involving a cylinder of square cross-section with arbitrary angular orientations, requires the application

of a body-fitted co-ordinate calculation approach. While previous studies using rectangular grids provide some indication of the level of grid refinement required to resolve the present unsteady flow, they have all been performed for numerical schemes that were second-order-accurate in space but only first-order-accurate in time. Since the findings of those studies do not necessarily apply to the present higher-order curvilinear finite difference scheme, an independent and fairly exhaustive investigation of its grid dependence characteristics has been performed. In this regard, references in the text to 'good' agreement are supported by *quantitative* statements where appropriate.

2. THE NUMERICAL PROCEDURE

Details concerning the derivation of finite difference approximations for the conservation equations and of the numerical procedure implemented for solving them are provided in Reference 35. Except for the more general curvilinear co-ordinate capability of the present numerical procedure, modelled along the lines of Schuh *et al.*,[36] the calculation methodology closely parallels that of the CUTEFLOWS algorithm described by Schuler *et al.*[37] This section summarizes the major points of interest.

2.1. Conservation equations and boundary conditions

This study assumes a constant property (non-buoyant), unsteady but streamlined, two-dimensional flow over the parameter ranges explored. The relevant continuity, momentum and energy equations in arbitrary curvilinear co-ordinates (ξ^1, ξ^2) are respectively

$$\frac{\partial(\rho J U^i)}{\partial \xi^i} = 0, \tag{1}$$

$$\frac{\partial(\rho J u)}{\partial t} + (\rho J U^i u)_{\xi^i} = -\left(y_{\xi^2} p\right)_{\xi^1} + \left(y_{\xi^1} p\right)_{\xi^2} + \mu\left(J g^{ij} u_{\xi^j}\right)_{\xi^i}, \tag{2a}$$

$$\frac{\partial(\rho J v)}{\partial t} + (\rho J U^i v)_{\xi^i} = +\left(x_{\xi^2} p\right)_{\xi^1} - \left(x_{\xi^1} p\right)_{\xi^2} + \mu\left(J g^{ij} v_{\xi^j}\right)_{\xi^i}, \tag{2b}$$

$$\frac{\partial(\rho c_p J T)}{\partial t} + (\rho c_p J U^i T)_{\xi^i} = k\left(J g^{ij} T_{\xi^j}\right)_{\xi^i}. \tag{3}$$

While the symbols in the above equations are defined in the Appendix, the reader is reminded that (u, v) are the (x, y) Cartesian velocity components, the superscripts i and j denote contravariant components, the subscripts ξ^i and ξ^j represent partial derivatives with respect to these curvilinear co-ordinates and the summation convention on repeated indices applies throughout. The contravariant velocity component U^i is defined by the dot product $U^i = \mathbf{u} \cdot \mathbf{a}^i$, where $\mathbf{a}^i$ is the contravariant base vector given by $\mathbf{a}^i = \nabla \xi^i$ $(i = 1, 2)$ and ∇ is the gradient operator.

Equations (1)–(3) are elliptic in space and parabolic in time. They require appropriately formulated boundary conditions for their solution. With reference to Figure 1, the boundaries of the solution domain consist of the four surfaces of the square cylinder, the two surfaces (top and bottom walls) of the channel and the inlet and outlet planes of the channel. No-slip, impermeable wall velocity boundary conditions and constant temperature boundary conditions for the non-isothermal flows were imposed on the cylinder and channel surfaces. Uniform velocity (and temperature) profiles were specified at the inlet plane to yield the flow Reynolds numbers of interest. The translating velocities of the channel walls were fixed to the inlet plane velocity condition. At the outlet plane $\partial u/\partial t + c(\partial u/\partial x) = 0$ and $\partial(v, T)/\partial x = 0$ were specified. The former is an open boundary

condition for u, where c is the speed of the u-wave, a quantity that is positive or zero. This condition has been employed and carefully discussed by, for example, Han *et al.*,[38] Arnal *et al.*,[33] Treidler[29] and Tatsutani *et al.*[30] It allows the correct development of the unsteady flow in an obstructed channel of finite length by permitting shear-induced vortical flow structures to pass through the outlet plane of the channel without reflecting waves at this boundary. In all cases the values of velocity and temperature prescribed at the channel inlet plane were used as the initial field values for the calculation conditions at the lowest Reynolds number. The calculated flow and temperature fields obtained at one Reynolds number were used as the initial conditions for calculations at the next highest Reynolds number.

2.2. Finite difference approximations and solution methodology

Finite difference forms of the transport equations are obtained by control volume integration on staggered grids as done by Humphrey[39] for toroidal co-ordinates, but here derived for arbitrary curvilinear co-ordinates. Second-order-accurate schemes are used to approximate the diffusion and pressure gradient terms (using central differencing) and the convection terms (using the flux-limited form of the QUICK scheme proposed by Leonard[40,41] to avoid over/undershooting in the calculations). The semidiscrete transport equations so derived are then solved for the contravariant velocity components and temperature using a time-explicit, second-order (predictor–corrector) Runge–Kutta method. By forcing the velocity field at each time step to obey the continuity equation, the solution to the pressure field is also obtained. In this regard, CUTEFLOWS employs the conjugate gradient method[42] to solve the system of algebraic equations yielding the pressure field. In this study it was found that the modified strongly implicit method of Schneider and Zedan,[43] also employed by Arnal *et al.*[33] in a flow configuration similar to the present one, had essentially the same speed of solution as the conjugate gradient method but was less sensitive to singularities in the pressure coefficient matrix. For this reason it was the preferred method for calculating pressure. Because momentum and energy are decoupled in the present problem, the temperature field is calculated at the end of each time step after the velocity field has been obtained.

2.3. Grid considerations, algorithm testing and computational requirements

The curvilinear grids used in this study were generated via a multiblock grid generation procedure. In this approach the calculation domain is subdivided into blocks and grid distributions are prescribed

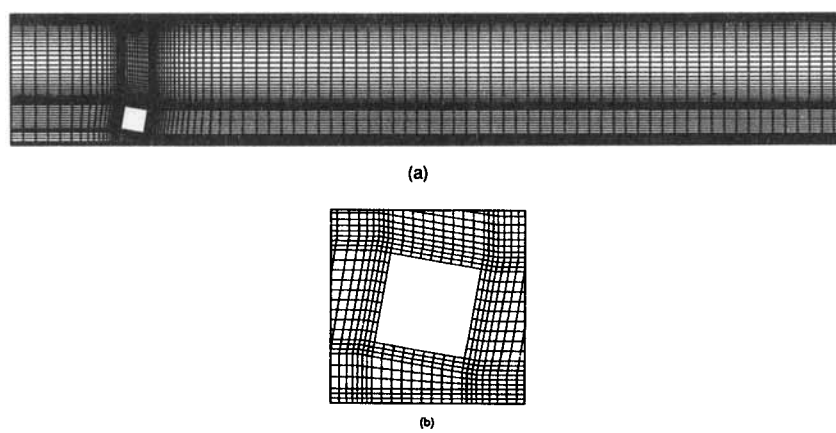

Figure 2. Typical refinement and distribution of the numerical grid with (99, 55) nodes used to calculate the two-dimensional flow of Figure 1 in the case with $\alpha = 10°$, $h/H = 0{\cdot}192$ ($g/d = 0{\cdot}5$) and $d/H = 0{\cdot}192$: (a) complete grid; (b) grid near the cylinder

along the block boundaries. The algebraic method is then used to generate the grids inside each block and the resulting overall grid is finally smoothed out using the elliptic method. (See Reference 35 and 44 for details of practical implementation.) Figure 2 shows an example of the refinement and distribution of a grid used to calculate the flow configuration of Figure 1.

The goodness of the numerical procedure was verified by reproducing the flow and heat transfer results of five test cases, here deliberately calculated on non-uniform curvilinear grids over extensive ranges of the respective flow parameters. The calculations correspond to steady and unsteady flows. The steady solutions are for the wall-driven flow in a square enclosure,[45] the buoyancy-driven flow in a square enclosure[46] and the flow over a backward-facing step in a channel.[33,47,48] The unsteady solutions are for the flow past a square cylinder in a freestream[4,5,29,32,33] and the flow past a cylinder of variable orientation in a channel with fixed walls.[35] Of the latter two cases, the first was calculated on a non-uniform rectangular grid.

Detailed comparisons with the data from these references are provided in Reference 35 and discussed in depth in Reference 17. Except for the case of the backward-facing step, all the results compared (velocity profiles, streamlines, vorticity and temperature contours, drag coefficients, Strouhal numbers and particle trajectories) were in good agreement for the other four cases. From these test case results and the additional information provided by Davis *et al.*,[31] Arnal *et al.*[33] and Suzuki *et al.*,[32] it was possible to quantify the levels of grid and time step refinements required to resolve the flow of primary interest to this work. In this regard the following three points are important to note.

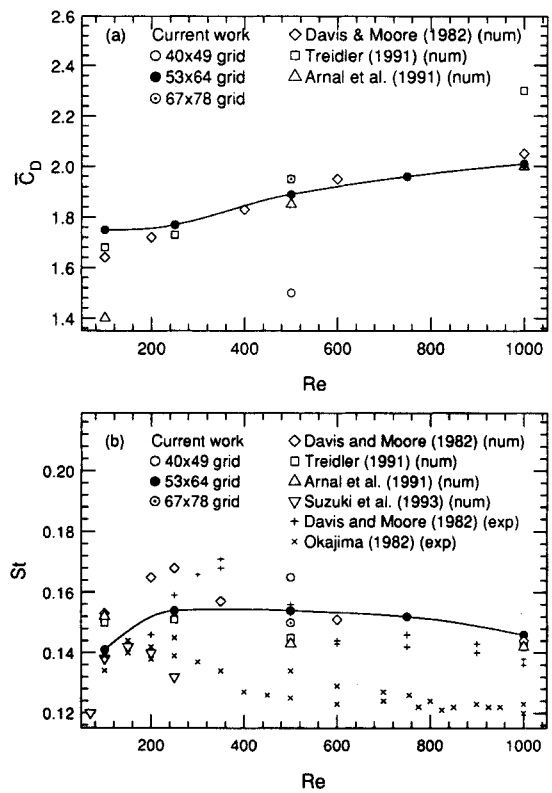

Figure 3. Comparison among (a) drag coefficient, $\bar{C}_D$, and (b) Strouhal number, St, results for the flow past a square cylinder in a free stream

(1) A comparison between present calculations and the results of others for the average drag coefficient and the Strouhal number of the flow past a square cylinder in a freestream are provided in Figure 3. Present predictions, initially made using a non-uniform rectangular (53, 64) grid with Re_Δ ranging from 10 to 100, depending on Re, yielded $\bar{C}_D$ results in good agreement with the calculations of Davis and Moore[4] over the entire range of Reynolds numbers ($100 < Re < 1000$). (For this flow the definition of the Reynolds number is based on the cylinder diameter and the freestream velocity.) In contrast, the results for St differ significantly, with the measurements by Okajima[5] and Davis and Moore[4] showing discrepancies ranging from 14% to 21% for $Re > 250$. Similarly, the calculations of Davis and Moore[4] and Suzuki *et al.*[32] differ by as much as 25% for $Re < 300$. The present results fall between those of Davis and Moore[4] and Suzuki *et al.*[32] for $Re < 300$ and are in close agreement with the experimental and numerical results of Davis and Moore[4] for $Re > 300$. Except for the work by Suzuki *et al.*,[32] for which the details of the boundary conditions are not available, the other calculations for this case were performed with symmetry plane boundary conditions imposed along parallel fictitious sliding surfaces located six cylinder diameters above and below the cylinder centre.

Suzuki *et al.*[32] have suggested that the large differences between the respective measurements of St by Okajima[5] and Davis and Moore[4] may be partly due to the different velocity fluctuation levels in the approaching flows. That *high* values of turbulence intensity (ranging between 5% and 20%) are capable of significantly altering the average drag, lift and Strouhal number of the flow past a cylinder of square cross-section has been documented experimentally by, for example, Cheng *et al.*[11] However, the RMS fluctuations in the experiments of Okajima[5] and Davis and Moore[4] are respectively quoted as being 0·5% and 0·05% of the freestream velocities. Berger and Wille[2] discuss the influence of approaching flow velocity fluctuations on vortex shedding from *circular* cylinders for low Reynolds number ($40 < Re < 170$ approximately). They conclude that '... below $Re = 100$, a vortex-street configuration of extreme regularity and stable phase relation exists ... . Above $Re = 90$, the regular street mode exists only at extremely low turbulence levels of the onflow, less than 0·05 percent. At higher turbulence levels only the high-speed mode could be found to be stable. Within a certain limit of turbulence level, 0·05–0·07 percent, both vortex-street configurations are metastable and, from time to time, change back and forth from one to the other'.

Even though the observations of Berger and Wille[2] are for cylinders of circular cross-section, it is conceivable that at *low* Reynolds numbers ($Re < 200$) Okajima[5] and Davis and Moore[4] could have observed different modes of oscillation frequency as a result of the different velocity fluctuation levels in their respective experiments. However, this is the range over which their data differ the *least*, by less than 3% compared with 14%–21% for $Re > 250$! Given that the differences in frequency between the two modes of oscillation referred to by Berger and Wille[2] are of the order of 5% and that these modes arise at low Reynolds numbers, it seems unlikely that the much larger differences in frequency observed at much larger Reynolds numbers between the data of Okajima[5] and Davis and Moore[4] can be principally attributed to the different velocity fluctuations levels in the respective experiments. Since Okajima[5] and Davis and Moore[4] were both able to determine their respective Strouhal number data to within ±2%–5% RMS uncertainty, it is suggested that at least one of the two experiments was affected by unknown systematic error(s).

(2) Additional calculations were performed for the flow past a square cylinder in a freestream at $Re = 500$ using non-uniform grids with (40, 49) and (67, 78) nodes. Results for $\bar{C}_D$ and St, also plotted in Figure 3, can be fitted to a polynomial to yield the (extrapolated) grid-independent values $\bar{C}_D = 2.1$ and $St = 0{\cdot}144$. From this it is possible to show that $\bar{C}_D$ and St calculated on the medium (53, 64) grid are both within 7%–11% of their respective grid-independent results, while the values obtained on the finest (67, 78) grid are within 4%–7%. A consideration of these numbers leads to the conclusion that to obtain $\bar{C}_D$ and St results to within 1%–2% of their grid-independent values, grids more refined than

(180, 220) nodes would be necessary. Unfortunately, for the number of cases planned for calculation in this study, such grid densities were simply unaffordable and a compromise was reached.

(3) To further verify the ability of the numerical procedure to reproduce the features of the flow configuration of primary interest here, shown in Figure 1, the fixed wall channel flow apparatus of Tatsutani *et al.*[30] was modified as explained in Reference 35 to visualize the flow past a single square cylinder with the following characteristics: $\alpha = 0°$, 10° and 20°, $h/H = 0{\cdot}273$, $d/H = 0{\cdot}182$, $w/d = 1$, $W/H = 12{\cdot}27$, $Re = 100$–1000. The experimental flow conditions and the method of visualization were reproduced numerically with the channel length set to $W/H = 6{\cdot}44$, for calculation economy, to yield calculated streaklines in good qualitative agreement with the ones photographed.[35]

Three instances of the flow visualized numerically on a (99, 55) grid are shown in Figure 4. These reveal an unexpected result which was observed for all the experimental and numerical conditions of this case: that the less intense vortex detaching from the bottom surface of the cylinder wraps around the more intense vortex detaching from the top surface as the flow moves downstream. Such behaviour has not been observed in previous studies with the cylinder located symmetrically on the channel midplane (i.e. with $\alpha = 0°$). It is the result of the flow asymmetry induced by rotating the cylinder to an angle $\alpha > 0°$ and/or by displacing it from the channel midplane. The predictions of Suzuki *et al.*,[32] for the flow past a square cylinder with $\alpha = 0°$ at various distances from the fixed walls of a channel, do not show this 'vortex-wrapping' phenomenon either. This is attributed to the larger cylinder–channel

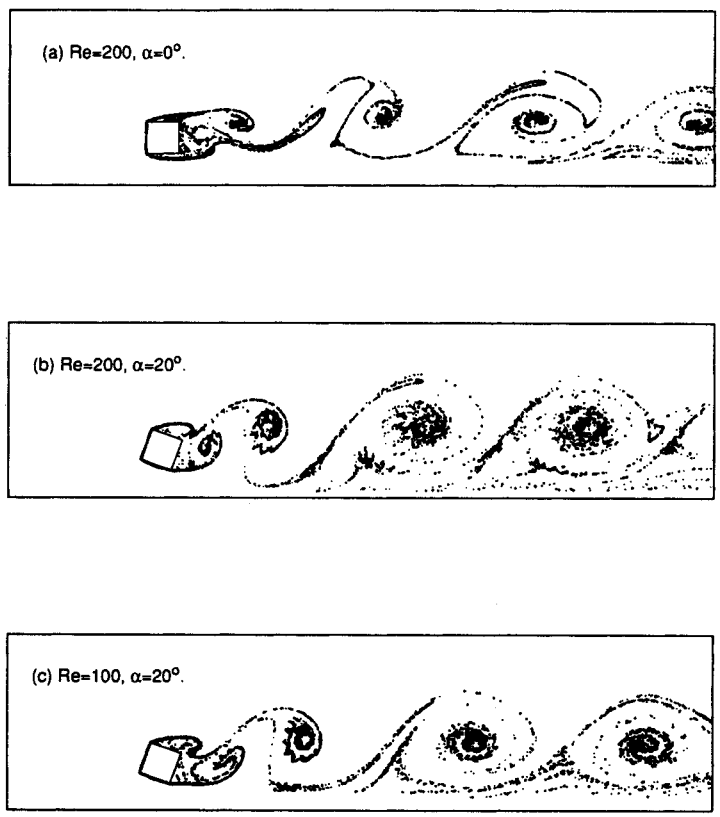

Figure 4. Instantaneous numerically calculated streaklines for the experimental conditions of this work corresponding to the flow past a square cylinder in a channel with fixed walls: $h/H = 0{\cdot}273$ ($g/d = 1{\cdot}0$), $d/H = 0{\cdot}182$ and $W/H = 6{\cdot}44$ ($W/H = 12{\cdot}27$ in the experiment)

Table II. Average values of the measured (St_m) and calculated (St_c) Strouhal numbers for the flow past a cylinder of square cross-section in a channel with fixed walls and in a free-stream respectively. The channel flow conditions are $h/H=0{\cdot}273$ ($g/d=1{\cdot}0$), $d/H=0{\cdot}182$ and $w/d=1$. The values of St_m in the channel are from the present work; those in the freestream are averaged from the two data sets in Reference 4. The RMS uncertainty in St_m is 5% approximately. All the values of St_c are from this work and are estimated to be accurate to within 7%

Re		$\alpha=0°$	$\alpha=10°$	$\alpha=20°$	Freestream
200	St_m	0·235	0·242	0·228	0·144
	St_c	0·230	0·220	0·212	0·150 (interpolated)
600	St_m	0·188	0·242	0·211	0·144
	St_c	0·195	0·232	0·186	0·153 (interpolated)
1000	St_m	0·151	0·228	0·194	0·137
	St_c	0·180	0·233	0·190	0·146

obstruction ratio explored by them, $d/H=0{\cdot}3$, compared with the present value of 0·182. For values of $Re<400$ the present experimental flow was essentially two-dimensional about the vertical symmetry plane of the channel, i.e. the plane dividing the cylinder into two equal lengths. For $Re>600$, flow three-dimensionally appeared within $5d$ to $10d$ lengths downstream of the cylinder.

A quantitative comparison between measured and calculated values of *St*, provided in Table II, shows that agreement ranges between 2% and 10% approximately, except for the values at $Re=1000$ with $\alpha=0°$ which differ by 19%. (The RMS uncertainty in the experimental value of *St* is estimated to be 5% approximately.) Both the measurements and calculations show that for fixed α, *St* tends to decrease with increasing *Re*, while for fixed *Re*, *St* tends to maximize at an orientation angle between $\alpha=0°$ and 20°.

3. RESULTS

Table I shows the geometrical and dynamical conditions investigated for the sliding wall flow configuration of Figure 1. With reference to that figure, $W/d=33{\cdot}5$, $L/d=4{\cdot}5$ and $d/H=0{\cdot}192$ were set in all the calculations. An example of the non-uniform curvilinear grids used for a cylinder with $h/H=0{\cdot}192$ and $\alpha=10°$ is shown in Figure 2. All the cases presented under this heading were calculated using grids with (99, 55) nodes to obtain node densities comparable with the finest employed in the test cases discussed above. The grid Reynolds numbers ranged from $Re_\Delta=5$ to 80 for the values of *Re* investigated. From the extensive tests performed, it is estimated that the level of grid refinement imposed in the vicinity of the cylinder and channel surfaces allowed predictions of the drag, lift and Nusselt number to better than 7% and of the Strouhal number to better than 4% of the grid-independent values of these quantities over the parameter ranges investigated.

The calculations were performed non-dimensionally. For the forced convection heat transfer cases a Prandtl number $Pr=0{\cdot}71$, corresponding to air, was assumed. Two heat transfer conditions were investigated. In one case the cylinder surfaces were uniformly fixed at a higher temperature than the channel walls and inlet flow, the latter two being at the same temperature. In the other case the channel walls were uniformly fixed at a higher temperature than the cylinder surfaces and inlet flow, the latter two being at the same temperature. In a calculation sequence to investigate the effects on the flow of a particular choice of parameters, the first calculation at the lowest Reynolds number was started with the initial velocity (and temperature) fields specified to the values at the channel inlet plane.

Calculations at the next value of the Reynolds number were then started from the converged fields obtained at the previous setting of that parameter. A numerical run was taken to its steady or periodic state, as determined by monitoring the time rate of change of the drag and lift coefficients. Within each time step in a numerical run the criterion for convergence was that the residual mass balance should be less than a non-dimensional value of 10^{-7}. In selected cases, finite perturbations deliberately imposed on a converged flow field were observed to dampen out to yield field solutions identical with the unperturbed ones.

The main findings, pertaining to the effects of h/H, α and Re on the flow as well as some results for heat transfer, are discussed below. Space constraints require that attention be restricted to a representative sample of the many plots available in Reference 35 for values of the Reynolds number equal to 100, 500 and 1000.

3.1. Parameter effects on the flow

While the parameter h/H in Table I unambiguously fixes the location of the cylinder centre relative to the channel walls, the quantity $g/d=(h-d/2)/d$ (also given in Table I) provides a more readily visualized dimensionless measure of the minimum distance between the bottom cylinder surface and the channel wall. This measure is exact for $\alpha=0°$ and in error by a few per cent for $\alpha=10°$ and 20°.

Figures 5 and 6 show plots of the instantaneous streamlines, vorticity and streaklines in flows with $\alpha=0°$ and 10° respectively for $Re=500$ and $g/d=1{\cdot}0$. Figure 7 shows the corresponding plots for $\alpha=10°$ in a flow with $Re=500$ and $g/d=0{\cdot}2$. The first pair of figures illustrates the effect of α, while the second pair shows the effect of g/d. Plots of the time-averaged drag and lift coefficients as well as the Strouhal number for all the cases explored are provided in Figures 8–10.[f5]

Except for two flow configurations at $Re=100$ with the cylinder very near the channel wall ($g/d=0{\cdot}2$ with $\alpha=0°$ and 10° respectively), the rest yielded unsteady solutions as evidenced by the alternating shedding of vortices from the top and bottom surfaces of the cylinder. The vorticity plots of Figures 5 and 6 show especially clearly that the flow approaching the cylinder comes to rest at a stagnation point on its upstream surface, the location of which depends on α. As expected,[49] with increasing α the stagnation point moves towards the corner of the cylinder projecting furthest into the approaching flow. At all three values of Re, flow separation occurred at the upstream corners of the cylinder. With increasing α the recirculation region above the top surface of the cylinder grew modestly

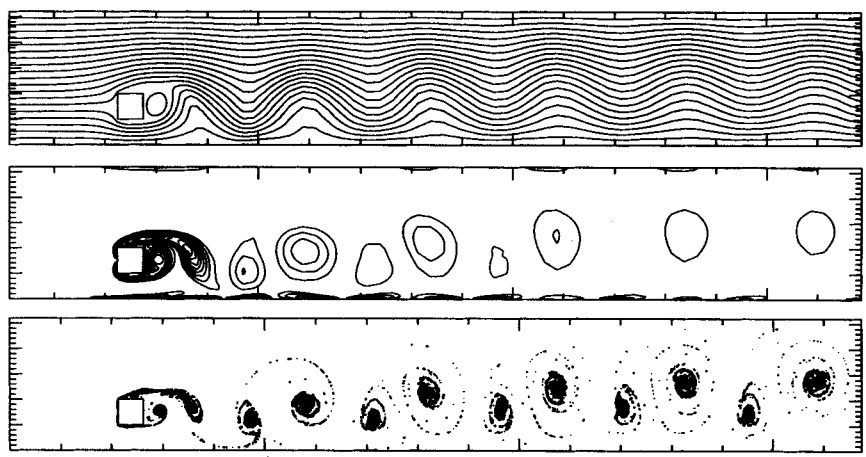

Figure 5. Instantaneous streamlines (top), vorticity contours (middle) and particle streaklines (bottom) for the flow past a square cylinder in a channel with sliding walls and $\alpha=0°$, $h/H=0{\cdot}288$ ($g/d=1{\cdot}0$), $d/H=0{\cdot}192$, $Re=500$

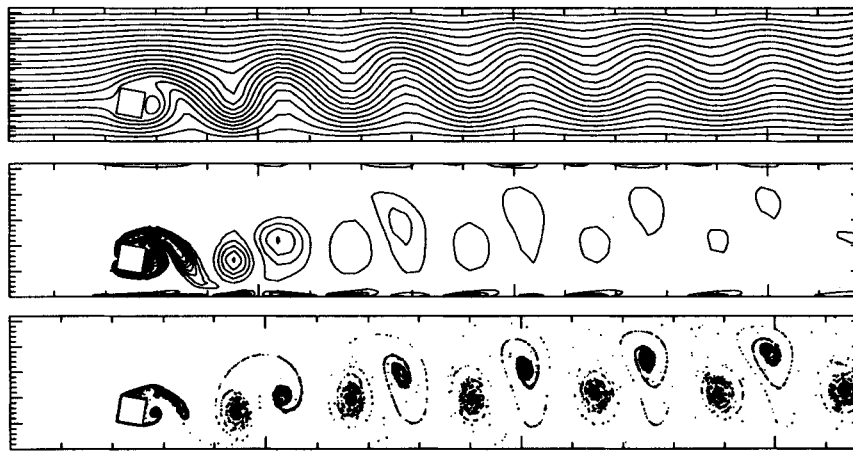

Figure 6. Same as Figure 5 with $\alpha = 10°$, $h/H = 0{\cdot}288$ ($g/d = 1{\cdot}0$), $d/H = 0{\cdot}192$, $Re = 500$

in size while that below the bottom surface became substantially smaller. For Re and α fixed, reducing the gap size (g/d) further decreased the size of the bottom recirculating flow region relative to the top.

From the work of Arnal *et al.*[33] the present flow is expected to undergo a transition from steady to unsteady motion at some characteristic value of Re which depends on the geometrical parameters. A calculation performed with $Re = 100$ for the conditions of Figure 7 revealed a steady flow with a pair of vortices fixed in the wake of the cylinder. At some value of Re between 100 and 500 the flow became sufficiently unsteady to display the vortex-shedding phenomenon. (Suzuki *et al.*[32] have also observed the transition from a steady flow to an unsteady vortex-shedding flow for a square cylinder with $\alpha = 0°$ and $d/H = 0{\cdot}3$ at $Re = 150$ in a channel with *fixed* walls as it is displaced from $g/d = 0{\cdot}17$ to $0{\cdot}58$.) In all the present unsteady flow cases the vortices alternately shed from the top and bottom surfaces of the cylinder tended to move towards and beyond the channel midplane. The vortex shed from the top surface of the cylinder was always more intense than the one shed from the bottom, the difference in circulation intensity increasing with increasing α and decreasing g/d. However, the 'vortex-wrapping' phenomenon discussed under point (3) in Section 2.3 was never observed and, because of the sliding

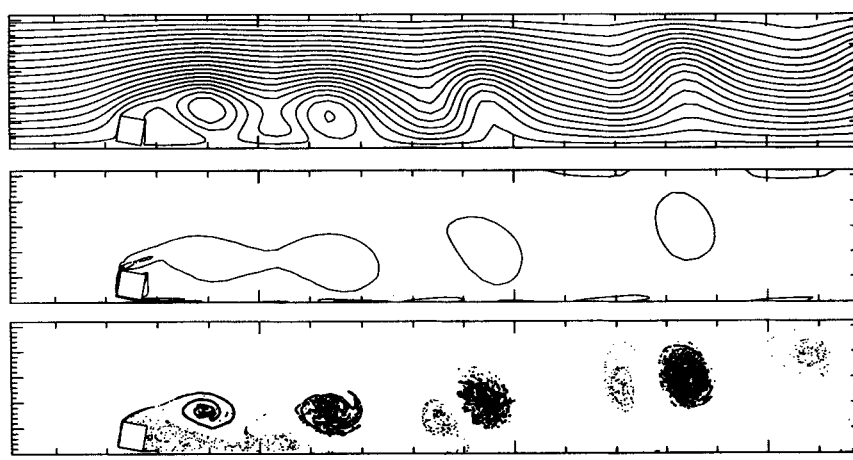

Figure 7. Same as Figure 5 with $\alpha = 10°$, $h/H = 0{\cdot}135$ ($g/d = 0{\cdot}2$), $d/H = 0{\cdot}192$, $Re = 500$

wall boundary condition, none of the cases calculated yielded regions of flow reversal along the channel walls as observed in the fixed wall channel of Davis *et al.*[31]

Instantaneous values of the drag and lift coefficients, available in Reference 35, were obtained by integrating the contributions of the shear stress and pressure distributions acting along the x- and y-co-ordinate directions on the cylinder surfaces. Time records of these two quantities were then averaged over approximately 20 cycles to obtain values for the average drag, $\bar{C}_D$, and lift, $\bar{C}_L$, coefficients. The Strouhal number was determined from the time variations in $\bar{C}_D$ and $\bar{C}_L$. The numbers obtained were in agreement with corresponding values determined from velocity component time records. All these results are plotted in Figures 8–10, where lines have been drawn through the points in the figures to facilitate interpretation. The lines do not necessarily imply the detailed interpoint variation of the quantities plotted.

All the values of $\bar{C}_D$ in Figure 8 exceed those corresponding to the case of freestream flow by a factor ranging from 1·25 to 2·1 at $Re = 100$ and from 1·35 to 2·4 at $Re = 1000$. They also exceed the values of $\bar{C}_D$ corresponding to a cylinder mounted on a fixed wall. This is due to the sliding walls condition. At $Re = 100$ the trends in the data are clear for all gap sizes, with $\bar{C}_D$ increasing with increasing α and decreasing g/d. In addition, for the two larger gap sizes ($g/d = 0{\cdot}5$ and 1) $\bar{C}_D$ is observed to also increase with increasing Re. In contrast, for the smallest gap size ($g/d = 0{\cdot}2$) $\bar{C}_D$ *decreases* with increasing Re for both angular orientations. The result is that as of $Re > 160$, approximately, with α fixed the value of $\bar{C}_D$ maximizes somewhere between $g/d = 0{\cdot}2$ and 1. For values of $Re > 400$ this maximum appears to lie close to $g/d = 0{\cdot}5$.

The average lift coefficient for a square cylinder with $\alpha = 0°$ in a freestream is zero. Figure 9 shows the results for a cylinder located asymmetrically between the sliding walls of a channel. For all the configurations explored, $\bar{C}_L$ initially decreases with increasing Re but subsequently increases (modestly) to yield minima at values of Re which depend on the settings of the geometrical parameters.

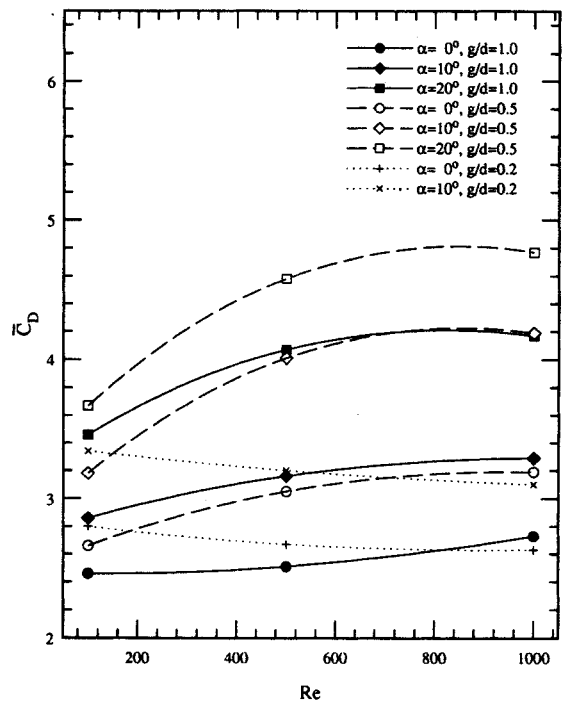

Figure 8. Average drag coefficient $\bar{C}_D$ as a function of Re for the conditions investigated for the flow past a square cylinder in a channel with sliding walls

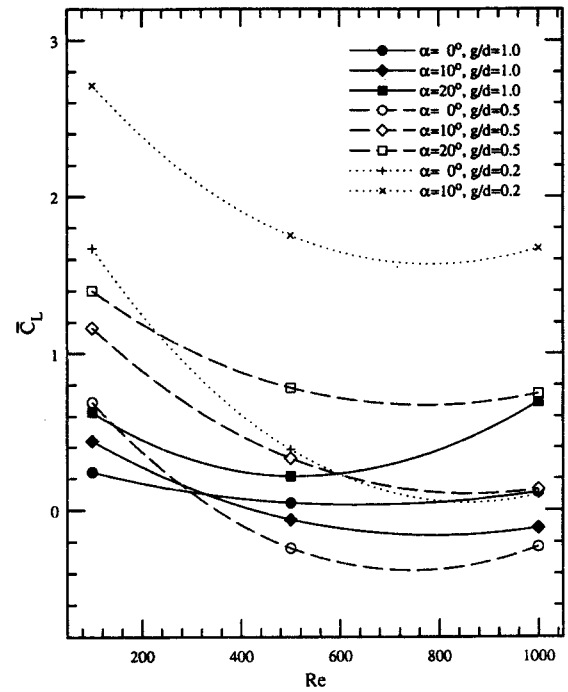

Figure 9. Average lift coefficient $\bar{C}_L$ as a function of *Re* for the conditions investigated for the flow past a square cylinder in a channel with sliding walls

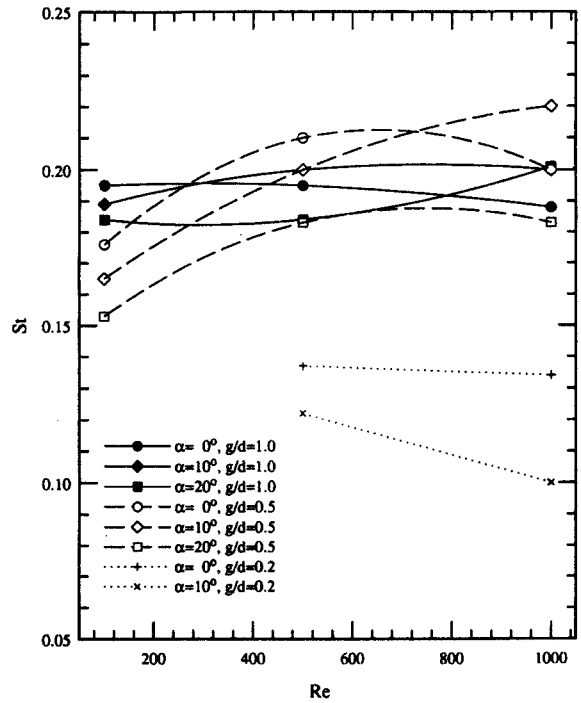

Figure 10. Strouhal number *St* as a function of *Re* for the conditions investigated for the flow past a square cylinder in a channel with sliding walls

As for $\bar{C}_D$, at $Re = 100$ the variations in $\bar{C}_L$ are clear, the value of this quantity increasing with increasing α and decreasing g/d. Although the crossing over of the $\bar{C}_L$ curves at higher Re renders physical interpretation difficult, it is clear that the increase in $\bar{C}_L$ due to increasing α is more pronounced for small values of g/d than for large. Again this is attributed to the sliding walls condition. The $\bar{C}_L$ data corresponding to $\alpha = 0°$ show that for $Re > 280$, approximately, this quantity minimizes with respect to g/d. Similarly the $\bar{C}_L$ data corresponding to $g/d = 1$ show that for $Re > 350$, approximately, this quantity also minimizes with respect to α. *Negative* values of $\bar{C}_L$ are predicted in the range $500 < Re < 1000$ for cylinders with $\alpha = 10°$ and $g/d = 1$, and with $\alpha = 0°$ and $g/d = 0{\cdot}5$.

The Strouhal number calculations plotted in Figure 10 show that this quantity is relatively insensitive to variations in Re and α for the largest gap size setting, $g/d = 1$. A much stronger dependence on these two parameters, with St ranging between 0·15 and 0·22, arises for the cases with $g/d = 0{\cdot}5$. With a decrease in g/d from 0·5 to 0·2 the values of St are markedly reduced, by as much as 45%, relative to the larger gap settings. For $g/d = 0{\cdot}2$ the larger of the two orientation angles ($\alpha = 20°$) yields the smallest value of all the Strouhal numbers, $St = 0{\cdot}1$ at $Re = 1000$. This near-wall damping of the flow oscillations, characteristic of both fixed and sliding walls, is in keeping with the earlier findings of Arnal *et al.*[33] The values of St calculated for $g/d = 1$ and 0·5 are 5%–55% larger than those predicted at the corresponding Re for the case of freestream flow, while the values calculated for $g/d = 0{\cdot}2$ are 5%–30% smaller.

3.2. *Parameter effects on heat transfer*

Instantaneous temperature contours and streamlines are shown in Figure 11 for the case of a cylinder with $\alpha = 0°$ and $g/d = 0{\cdot}5$ in a channel where the sliding walls are heated relative to the cylinder and inlet flow. Comparing the top and middle figures shows the marked effect of vortex shedding on the temperature distribution in the channel. The shedding of vortices with alternating sense of rotation and relatively low translational velocity works to periodically thin the wall thermal layers. In this regard the temperature contours show that both channel walls are affected by the vortical flow. This is further supported by the plots of the instantaneous local Nusselt numbers for the walls, $Nu_w(x)$, provided in Figure 12. Vortex shedding induces local wall heat transfer rates that are up to four times larger along

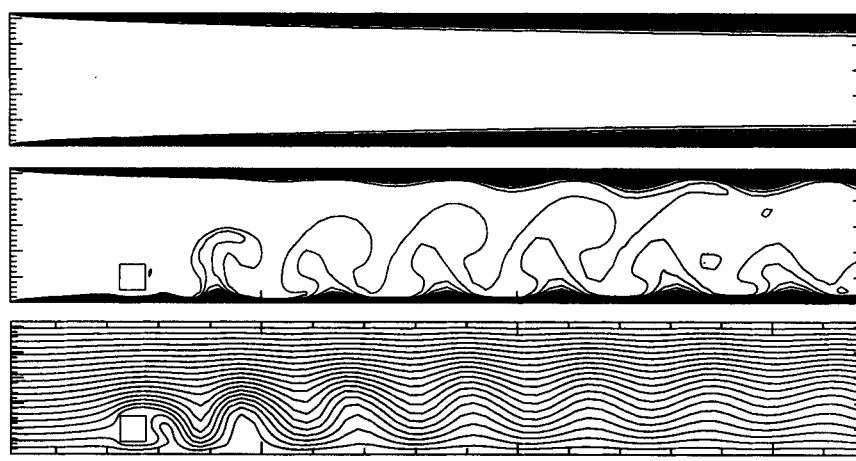

Figure 11. Instantaneous temperature contours and streamlines for the flow past a square cylinder in a channel with heated sliding walls and $\alpha = 0°$, $h/H = 0{\cdot}192$ ($g/d = 0{\cdot}5$), $d/H = 0{\cdot}192$, $Re = 500$. Temperature contours without the cylinder (top); temperature contours with the cylinder (middle); streamlines corresponding to middle plot (bottom)

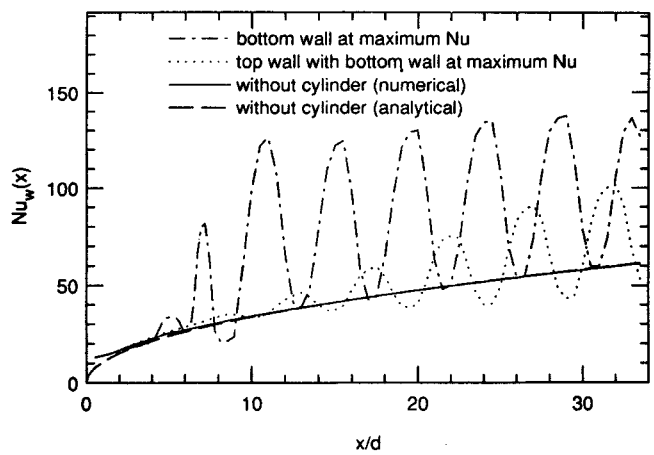

Figure 12. Instantaneous wall Nusselt number $Nu_w(x)$ for the flow past a square cylinder in a channel with heated sliding walls and $\alpha = 0°$, $h/H = 0{\cdot}192$ ($g/d = 0{\cdot}5$), $d/H = 0{\cdot}192$, $Re = 500$

the near-cylinder wall and 1·8 times larger along the far-cylinder wall relative to the corresponding unobstructed flow. The plot also shows excellent agreement between the analytical solution of the unobstructed flow configuration, given by $Nu_w(x) = (Re_x\, Pr/\pi)^{1/2}$ with $Re_x = U_i x/\nu$, and present calculations.

The dependence of the overall time- and surface-averaged channel wall Nusselt numbers, $\overline{Nu}_w$, on the cylinder orientation angle was also examined.[35] For example, the results for the case with $g/d = 0{\cdot}5$ and $Re = 500$ showed a weak increase in $\overline{Nu}_w$, from 184 at $\alpha = 0°$ to 198 at 20° for the near-cylinder wall and from 134 at 0° to 144 at 20° for the far-cylinder wall, approximately. More notable was the difference between the average Nusselt numbers for the two walls, as expected from Figure 11.

Calculations for the case of a cylinder at a higher temperature than the channel walls and inlet flow were also performed with $g/d = 0{\cdot}5$ and $Re = 500$. Time-averaged values of the individual, $\overline{Nu}_j$, and

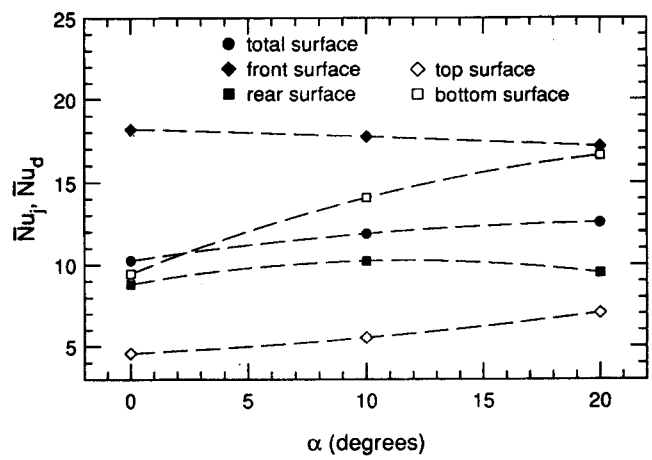

Figure 13. Time averages of individual, $\overline{Nu}_j$, and total surface, $\overline{Nu}_d$, Nusselt numbers as a function of orientation angle a for the flow past a heated square cylinder in a channel with sliding walls $h/H = 0{\cdot}192$ ($g/d = 0{\cdot}5$), $d/H = 0{\cdot}192$, $Re = 500$

total, $\overline{Nu}_d$, cylinder surface Nusselt numbers are plotted as a function of the orientation angle in Figure 13. For all values of α the upstream or 'front' surface of the cylinder presents the highest rate of heat transfer, but as α is increased the rate of heat transfer from the bottom surface closely approaches that from the front. For all values of α the lowest rate of heat transfer occurs along the top surface of the cylinder, where a recirculating flow region exists. The heat transfer from this surface increases modestly with increasing α. The rear surface of the cylinder is the second lowest in terms of heat transfer rate for all values of α. The average of the four surfaces shows a weak dependence on the orientation angle, increasing from $\overline{Nu}_d = 10.5$ at $\alpha = 0°$ to 12·5 at $\alpha = 20°$, approximately.

4. SUMMARY

The characteristics of the two-dimensional flow due to an immobile cylindrical obstruction of square cross-section located asymmetrically between the parallel sliding walls of a channel, in the range $100 < Re < 1000$ and with an obstruction ratio $d/H = 0{\cdot}192$, differ significantly and in a complicated manner from those of the same geometry with fixed walls or in a freestream. For a cylinder with wall distances $g/d = 0{\cdot}5$ and 1 in a channel with sliding walls the Strouhal number is larger than for a cylinder in a freestream over the range $0° < \alpha < 20°$. For $g/d = 0{\cdot}2$ the opposite is true and in agreement with the wall damping of vortex shedding predicted by Arnal *et al.*[33] for both fixed and sliding wall conditions. For values of $g/d = 0{\cdot}5$ and 0·2 in a sliding wall flow the Strouhal number generally decreases with increasing α over the range of Re explored. At these distances from the channel wall, increasing α significantly streamlines and stabilizes the fluid motion. Comparison of present results with the data of Arnal *et al.*[33] shows that the damping of flow oscillation is strongest for cylinders immediately adjacent to one of the channel walls. This is due to stabilization of the vortical motion in the wake of the cylinder, explained by those authors.

For a cylinder located asymmetrically in a channel, both the drag and lift coefficients differ from zero. Relative to a freestream flow or the flow in a channel with fixed walls, at the same Reynolds number the sliding wall condition increases the drag experienced by a cylinder for all the values of α and g/d of this work. Present results for sliding walls agree qualitatively with the data of Davis *et al.*[31] for fixed walls and show that drag increases with increasing Reynolds number and increasing blockage ratio d/H. (In the present flow configuration, increasing α effectively increases the blockage ratio.) Although the flow past a cylinder in a channel with g/d fixed and $\alpha = 20°$ is more streamlined than the flow for the same cylinder with $\alpha = 0°$, the larger local acceleration experienced by the fluid in the first case (with larger effective d/H) raises the skin friction and pressure drop contributions to drag. In general, irrespective of its angular orientation, moving a cylinder to an intermediate location near a sliding wall, say from $g/d = 1$ to 0·5, markedly increases the drag coefficient. This is because the sliding wall boundary condition maintains a higher value of streamwise component of momentum for the fluid approaching the cylinder at the intermediate location than it does for the fluid further away from the wall. The result is a larger momentum deficit incurred by the flow passing the cylinder at the intermediate location, which shows up as an increase in drag. However, in moving even nearer to the wall, from $g/d = 0{\cdot}5$ to 0·2, the drag is found to *decrease*. Now the sliding wall boundary condition assists the pressure recovery in the wake of the cylinder with an attendant reduction in drag. Finally, as shown by Arnal *et al.*,[33] placing the cylinder immediately adjacent to the sliding wall *increases* the drag. Now there is zero flow between the cylinder and the wall and all the fluid must pass over the cylinder in a highly irreversible manner. The associated pressure loss is responsible for the increase in drag.

Except for the narrow range of conditions shown in Figure 9, a cylinder located asymmetrically between the sliding walls of a channel generally experiences a positive lift coefficient, the largest

values of lift being associated with small g/d and large α. The largest lift-to-drag ratios in this work were also associated with the smallest g/d and largest α.

It was expected that vortex shedding from a cylinder should significantly affect the rate of heat transfer from the sliding walls of a channel. It is shown that a cylinder with an obstruction ratio $d/H = 0{\cdot}192$ at a wall distance $g/d = 0{\cdot}5$ can increase by as much as 40% the average heat transfer from the sliding wall nearest the cylinder relative to the same unobstructed flow. The vortices shed from a cylinder induce large time-dependent spatial variations in wall heat transfer which, along the near-cylinder wall, can reach values two to three times larger than those observed in the corresponding unobstructed flow. Over the range examined, the top and bottom surfaces of a heated cylinder showed the strongest dependence on the orientation angle, the average Nusselt numbers of these two surfaces increasing with α. For all α with $g/d = 0{\cdot}5$ the heat transfer from the bottom cylinder surface was about three times larger than from the top. However, the Nusselt number for the entire cylinder was only weakly dependent on α.

A limitation in this numerical analysis has been the assumption of a two- dimensional streamlined flow *downstream* of the cylinder. For the flow past a cylinder in a freestream or in a channel with fixed walls, with incresing Reynolds number one expects a two- to three-dimensional transition with the eventual appearance of turbulence. In the case of a freestream flow, numerical data for cylinders of circular cross-section support the establishment of the turbulent regime by $Re = 400$. To our knowledge the corresponding critical Reynolds number has not been established for square cylinders in channels with fixed or sliding walls. It seems reasonable to assume that for a small square cylinder in a large channel with fixed walls the critical Reynolds number should be near 400. *To what value, then, does the critical Reynolds number evolve if the walls of the channel are brought closer together and made to slide?* From the present results it is clear that the answer to this question depends on the obstruction ratio d/H, the cylinder–wall spacing g/d and the orientation angle α, with values of these parameters which stabilize the flow working to increase the critical Reynolds number. The resolution of this interesting question is not easy, since it requires precise experimentation with considerable attention to detail or accurate and computationally intensive three-dimensional calculations. It is the subject of continuing work.

ACKNOWLEDGEMENTS

This paper is dedicated to the memory of Ralph A. Seban. The investigation was performed under a grant received from the Computer Mechanics Laboratory of the Department of Mechanical Engineering at the University of California at Berkeley, with additional support provided by IBM (Austin and Boca Raton) under a grant to develop ICEME research methodologies. A scholarship received by G.L. from the K. C. Wong Education Foundation of Hong Kong is also gratefully acknowledged. We thank M. Bernstein and K. Tatsutani for their help in perfoming the flow visualization experiment of this work. The bulk of the calculations presented were performed on the UCB Campus CRAY X-MP/28, with computer time generously provided by the CRAY Corporation.

APPENDIX: NOMENCLATURE

$\mathbf{a}^i$	contravariant base vector
c_p	specific heat at constant pressure
C_D	drag coefficient, $(F_x/d)/\frac{1}{2}\rho U_i^2$
C_L	lift coefficient, $(F_y/d)/\frac{1}{2}\rho U_i^2$
d	diameter of the square cylinder of $d \times d$ cross-section
f	vortex-shedding frequency
F_x	drag force, aligned in x-co-ordinate direction

F_y lift force, aligned in y-co-ordinate direction
g distance between the square cylinder and nearest channel wall, $h - d/2$
g^{ij} contravariant metric tensor
h y-co-ordinate location of the centre of the square cylinder
h heat transfer coefficient, $-k(\partial T/\partial n)/\Delta T$
h_d heat transfer coefficient for the entire cylinder
h_j heat transfer coefficient for jth cylinder surface
$h_w(x)$ local heat transfer coefficient for a channel wall
h_w heat transfer coefficient for an entire channel wall
H distance between channel walls
J Jacobian of the co-ordinate transformation
k thermal conductivity
L x-co-ordinate location of the centre of the square cylinder
$\mathbf{n}$ unit vector normal to a surface
n co-ordinate normal to a surface
Nu_d Nusselt number for the entire cylinder, $h_d d/k$
Nu_j Nusselt number for jth cylinder surface, $h_j d/k$
$Nu_w(x)$ local Nusselt number for a channel wall, $h_w(x)x/k$
Nu_w Nusselt number for an entire channel wall, $h_w W/k$
p pressure
Pr Prandtl number, ν/λ
Re Reynolds number based on d, $U_i d/\nu$
Re_H Reynolds number based on H, $U_i H/\nu$
Re_Δ grid Reynolds number, $U_i \Delta x_{min}/\nu$
St Strouhal number, fd/U_i
t time
T temperature
$\mathbf{u}$ velocity vector
u x-velocity component
U^1 contravariant velocity component in the ξ^1-direction
U^2 contravariant velocity component in the ξ^2-direction
U_i bulk average or uniform fluid velocity at the channel inlet plane
U_w translating velocity of the channel walls
v y-velocity component
W length of the channel
x Cartesian co-ordinate
y Cartesian co-ordinate

Greek letters

α angular orientation of the square cylinder
Δ characteristic difference
λ thermal diffusivity, $k/\rho c_p$
μ dynamic viscosity
ν kinematic viscosity, μ/ρ
n^i ith curvilinear co-ordinate
ξ^1 streamwise curvilinear co-ordinate
ξ^2 transverse curvilinear co-ordinate
ρ density

Other

$-$ superscript denoting time-averaged value
min subscript denoting minimum value

REFERENCES

1. A. W. Marris, 'A review on vortex streets, periodic wakes, and induced vibration phenomena', *Trans. ASME, J. Basic Eng.*, **86**, 185–196 (1964).
2. E. Berger and R. Wille, 'Periodic flow phenomena', *Ann. Rev. Fluid Mech.*, **4**, 313–340 (1972).

3. V. T. Morgan, 'The overall convective heat transfer from smooth circular cylinders', *Adv. Heat Transfer*, **11**, 199–264 (1975).
4. R. W. Davis and E. F. Moore, 'A numerical study of vortex shedding from rectangles', *J. Fluid Mech.*, **116**, 474–506 (1982).
5. A. Okajima, 'Strouhal numbers of rectangular cylinders, *J. Fluid Mech.*, **123**, 379–398 (1982).
6. M. Braza, P. Chassaing and H. Ha Minh, 'Numerical study and physical analysis of the pressure and velocity fields in the near wake of a circular cylinder', *J. Fluid Mech.*, **165**, 79–130 (1986).
7. T. Igarashi, 'Characteristics of the flow around a square prism', *Bull. JSME*, **27**, 1858–1865 (1984).
8. T. Igarashi, 'Heat transfer from a square prism to an air stream', *Int. J. Heat Mass Transfer*, **28**, 175–181 (1985).
9. R. Franke, W. Rodi and B. Schonung, 'Numerical calculation of laminar vortex-shedding flow past cylinders', *J. Wind Eng. Ind. Aerodyn.*, **35**, 237–257 (1990).
10. P. M. Gresho and S. T. Chan, 'On the theory of semi-implicit projection methods for viscous incompressible flow and its implementation via a finite element method that also introduces a nearly-consistent mass matrix (Part 2: Implementation)', *Int. J. Numer Methods Fluids*, **11**, 621–660 (1990).
11. C. M. Cheng, P. C. Lu and R. H. Chen, 'Wind loads on square cylinders in homogeneous turbulent flows', *J. Wind Eng. Ind. Aerodyn.*, **44**, 739–749 (1992).
12. W. Rodi, 'On the simulation of turbulent flow past bluff bodies', *Proc. 1st Int. Symp. on Comp. Wind Eng.*, Tokyo, 1992.
13. A. Okajima, H. Ueno and H. Sakai, 'Numerical simulation of laminar and turbulent flows around rectangular cylinders', *Int. J. Numer. Methods Fluids*, **15**, 999–1012 (1992).
14. G. E. Karniadakis and G. S. Triantafyllou, 'Three-dimensional dynamics and transition to turbulence in the wakes of bluff objects', *J. Fluid Mech.*, **238**, 1–30 (1992).
15. M. Kato and B. E. Launder, 'The modelling of turbulent flow around stationary and vibrating square cylinders', *Proc. Ninth Symp. on Turbulent Shear Flows*, Kyoto, August 1993.
16. B. J. Vickery, 'Fluctuating lift and drag on a long cylinder of square cross-section in a smooth and a turbulent stream', *J. Fluid Mech.*, **25**, 481–494 (1966).
17. J. A. C. Humphrey and G. Li, 'Unsteady two-dimensional convective flow past a square obstruction placed asymmetrically between the parallel sliding walls of a channel', *Computer Mechanics Laboratory Report CML-93-015*, Mechanical Engineering Department, University of California at Berkeley, Berkeley, CA, 1993.
18. P. W. Bearman, 'Review–bluff body flows applicable to vehicle aerodynamics', *J. Fluids Eng.*, **102**, 265–274 (1980).
19. E. Marumo, K. Suzuki and T. Sato, 'A turbulent boundary layer disturbed by a cylinder', *J. Fluid Mech.*, **87**, 121–141 (1978).
20. E. Marumo, K. Suzuki and T. Sato, 'Turbulent heat transfer in a flat plate boundary layer disturbed by a cylinder', *Int. J. Heat Fluid Flow*, **6**, 249–255 (1985).
21. H. Suzuki, K. Suzuki and T. Sato, 'Dissimilarity between heat and momentum transfer in a turbulent boundary layer disturbed by a cylinder', *Int. J. Heat Mass Transfer*, **31**, 259–265 (1988).
22. K. Suzuki, H. Suzuki, Y. Kikkawa, H. Kigawa and Y. Kawaguchi, 'Study on a turbulent boundary layer disturbed by a cylinder–effect of cylinder size and position', in F. Durst, B. E. Launder, W. C. Reynolds, F. W. Schmidt and J. H. Whitelaw (eds), *Turbulent Shear Flows 7*, Springer, Berlin, 1991, pp. 119–135.
23. S. Taneda, 'Experimental investigation of vortex streets', *J. Phys. Soc. Jpn.*, **20**, 1714–1721 (1965).
24. P. W. Bearman and M. M. Zdravkovich, 'Flow around a circular cylinder near a plane boundary', *J. Fluid Mech.*, **89**, 33–47 (1978).
25. K. Kamemoto, Y. Oda and M. Aizawa, 'Characteristics of the flow around a bluff body near a plane surface', *Bull. JSME*, **27**, 1637–1643 (1984).
26. G. E. Karniadakis, B. B. Mikic and A. T. Patera, 'Minimum-dissipation transport enhancement by flow destabilization: Reynolds analogy revisited', *J. Fluid Mech.*, **192**, 365–391 (1988).
27. M. Yao, M. Nakatami and K. Suzuki, 'Flow visualization and heat transfer experiments in a duct with a staggered array of cylinders', *Exp. Thermal Fluid Sci.*, **2**, 193–200 (1989).
28. C. Amon and B. B. Mikic, 'Spectral element simulation of unsteady forced convective heat transfer: application to compact heat exchanger geometries', *Numer. Heat Transfer*, **19**, 1–19 (1991).
29. E. B. Treidler, 'An experimental and numerical investigation of flow past ribs in a channel', *Ph.D. Thesis*, University of California at Berkeley, Berkeley, CA, 1991.
30. K. Tatsutani, R. Devarakonda and J. A. C. Humphrey, 'Unsteady flow and heat transfer for cylinder pairs in a channel', *Int. J. Heat Mass Transfer*, **36**, 3311–3328 (1993).
31. R. W. Davis, E. F. Moore and L. P. Purtell, 'A numerical–experimental study of confined flow around rectangular cylinders', *Phys. Fluids*, **27**, 46–59 (1984).
32. H. Suzuki, I. Yoshiaki, N. Toshihiko, K. Fukutani and K. Suzuki, 'Unsteady flow in a channel obstructed by a square rod (crisscross motion of vortex)', *Int. J. Heat Fluid Flow*, **14**, 2–9 (1993).
33. M. P. Arnal, D. J. Goering and J. A. C. Humphrey, 'Vortex shedding from a bluff body on a sliding wall', *J. Fluids Eng.*, **113**, 384–398 (1991).
34. M. M. Zdravkovich, 'Smoke observations of the formation of a Karman vortex street', *J. Fluid Mech.*, **37**, 491–499 (1969).
35. G. Li, 'Calculations of flow and heat transfer for an obstruction between two sliding walls', *Ph.D. Thesis*, University of California at Berkeley, Berkeley, CA, 1992.
36. M. J. Schuh, C. A. Schuler and J. A. C. Humphrey, 'Numerical calculation of two-phase flow erosion in particle-laden gas flows past tubes', *AIChE J.*, **35**, 466–480 (1989).
37. C. A. Schuler, E. B. Treidler and J. A. C. Humphrey, 'CUTEFLOWS (computing unsteady three-dimensional elliptic flows): a user's guide', *Computer Mechanics Laboratory Report CML-91-001*, Mechanical Engineering Department, University of California at Berkeley, Berkeley, CA, 1991.

38. T. Y. Han, J. C. S. Meng and G. E. Innis, 'An open boundary condition for incompressible stratified flows', *J. Comput. Phys.*, **49**, 276–297 (1983).
39. J. A. C. Humphrey, 'Numerical calculation of developing laminar flow in pipes of arbitrary curvature radius', *Can. J. Chem. Eng.*, **56**, 151–164 (1978).
40. B. P. Leonard, 'A stable and accurate convective modeling procedure based on quadratic upstream interpolation', *Comput. Methods Appl. Mech. Eng.*, **19**, 59–98 (1979).
41. B. P. Leonard, 'A simple high-accuracy resolution program for convective modeling of discontinuity', *Int. J. Numer. Methods Fluids*, **8**, 1291–1318 (1988).
42. D. G. Luenberger, *Linear and Nonlinear Programming*, Addison-Wesley, Reading, MA, 1984.
43. G. E. Schneider and M. Zedan, 'A modified strongly implicit procedure for the numerical solution of field problems', *Numer. Heat Transfer*, **4**, 1–19 (1981).
44. J. F. Thompson, Z. U. Warsi and C. W. Mastin, *Numerical Grid Generation, Foundations and Applications*, North-Holland, New York, 1985.
45. U. Ghia, K. N. Ghia and C. T. Shin, 'High *Re* solutions for incompressible flow using the Navier–Stokes equations and a multigrid method', *J. Comput. Phys.*, **48**, 387–411 (1982).
46. G. De Vahl Davis, 'Natural convection of air in a square cavity: a bench mark numerical solution, *Int. J. Numer. Methods Fluids*, **3**, 249–264 (1983).
47. B. F. Armaly, F. Durst, J. C. F. Pereira and B. Schonung, 'Experimental and theoretical investigation of backward facing step flow', *J. Fluid Mech.*, **127**, 473–496 (1983).
48. N. N. Mansour, J. Kim and P. Moin, 'Computation of turbulent flows over a backward-facing step', *NASA TM 85851*, 1983.
49. L. M. Milne-Thomson, *Theoretical Hydrodynamics*, Macmillan, London, 1972.